The Abdus Salam
International Centre for Theoretical Physics

United Nations
Educational, Scientific and
Cultural Organization

IAEA
International Atomic Energy Agency

2146-21

Gribov-80 Memorial Workshop on Quantum Chromodynamics and Beyond'

26 - 28 May 2010

The Phenomenology of a Renormalized Pomeron

Uri Maor
Tel-Aviv University
Israel

GRIBOV-80 WORKSHOP
Trieste 26-28 May 2010

The Phenomenology of the renormalized pomeron

URI MAOR
Tel-Aviv University

An Abreviated Pre-History of the Pomeron

(1956) Pomeranchuk - equality of $\sigma_{tot}(pp)$ and $\sigma_{tot}(\bar{p}p)$ at high enough energies. Followed by studies with Gribov, Ioffe and Okun.

(1957) Regge - non relativistic theory in the complex J-plane.

(1960) Chew and Frautschi - Regge poles in high energy scattering.

(1961) Gribov-Pomeranchuk (latter changed to Pomeron) Regge Pole.

(1967) Gribov - Reggeon (Pomeron) field calculus.

At this time: $\alpha_P(t) = \alpha_P(0) + \alpha_P' t$

$\alpha_P(0) = 1.0$, $\alpha_P' = 0.25 - 0.30$ GeV^{-2}.

At high enough energies $\alpha_{I\!P}(0)$ is responsible for the energy dependence of σ_{tot} and the $t=0$ elastic and diffractive cross sections. $\alpha'_{I\!P}$ is responsible for the corresponding forward slopes, including shrinkage.

(1969) Bjorken, Feynman, Gribov - introduce the parton model.

(1970) Mueller - Generalized optical theorem, triple Regge (Pomeron) coupling.

(1970) Serpukhov - $\sigma_{tot}(Kp)$ is increasing with energy.

(1973) ISR (CERN) - $\sigma_{tot}(pp)$ is increasing with energy.

(1984) Donnachie and Landshoff - DL Regge parametrization $\alpha_{I\!P}(0) = 1+\Delta_{I\!P} = 1.08$, $\alpha'_{I\!P} = 0.25\ GeV^{-2}$. Reproduces well the total and elastic hadronic cross sections up to the Tevatron.

1. Introduction

The subject matter of this talk originates from studies carried out during the period spanning from the mid 70 ies to the mid 80 ies of the 20th century.
These studies were triggered by the common understanding that the simple Pomeron picture has to be replaced by a considerably more sophisticated presentation.

1) Serpukhov and CERN rising cross sections, epitomized by DL $\alpha_P > 0$, imply an eventual s-channel unitarity violation. Note that incorporating s-channel unitarity corrections is a model dependent procedure.
2) Mueller's triple Pomeron formalism leads to 2 fundamental observations coupled to the experimental determination that G_{3P} is not too small.
   2.1) There is a dynamic difference between low mass diffraction which is coupled to elastic scattering (Feinberg and Pomeranchuk (1953), Good and Walker (1960)) and high mass diffraction depending on G_{3P}

2.2) A large enough G_{3P} implies that Mueller's mechanism is just a Born term, to which we should add the more complicated multi Pomeron interactions (Schwimmer (1975), Kaidalov et. al (1986)).

3) Low (1975) and Nusinov (1975) pointed out the identity between the quantum numbers of the Pomeron and a colour singlet of 2 gluons. BFKL (1977) proceeded from the parton model to a detailed pQCD calculation in which the BFKL Pomeron is obtained at small x. Note that the soft Regge Pomeron is a simple moving pole in the J-plane while the hard BFKL Pomeron is a brance cut. HERA DIS data shows a smooth transition from a soft $\Delta_{I\!P}^{eff} \simeq 0.1$ to a hard $\Delta_{I\!P}^{eff} \simeq 0.4$ as a function of Q^2. $\Delta^{LO}_{BFKL} \simeq 0.5$ (fixed $\alpha_s = 0.2$). $\Delta^{NLO}_{BFKL} \simeq 0.13 - 0.18$. $\alpha'_{BFKL} = 0$.

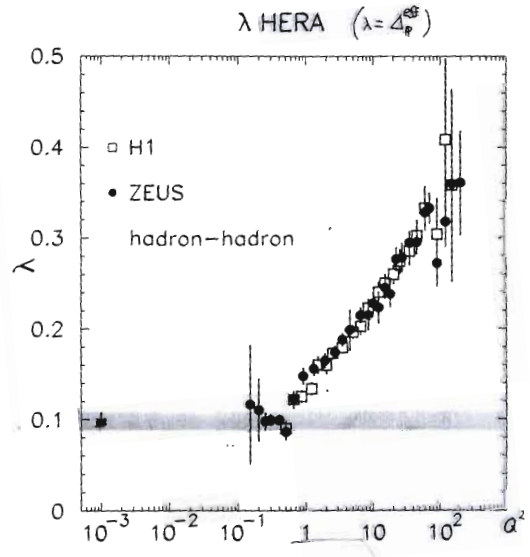

Given a traditional soft Pomeron input, $\alpha_{IP}(t) = \alpha_{IP}(0) + \alpha'_{IP} t$, I wish to assess its modifications due to s and t channel unitarity corrections. In the following I discuss:

1) Modellings and data reconstruction procedures. Experimentally, the total and elastic ($t \lesssim 0.5$ GeV) cross sections are compatible with the DL parametrization in the ISR-Tevatron energy range. The integrated diffractive cross sections (SD, DD) increase with energy very moderately. This behaviour is attributed to s-channel unitarity corrections (GLM (1999)). These experimental observations initiate an effective constraint on any viable model.

2) As it stands the theoretical relation between the soft and hard Pomerons is not clear. A very appealing consequence of Gribov (1969) is that we can construct a soft Pomeron formalism from hard ingredients. We wish to utilize this feature in a pQCD calculation.

3) The interplay between Pomeron theory and data analysis.

As we shall see, the critical ingredients of an updated Pomeron theory are initiated the corresponding output of the data analysis. An open problem is how do we consistently define diffraction. Recall that the Pomeron (soft or hard) does not transfer quantum information. As such a diffractive system of hadrons is separated from the other secondry hadrons by a larg rapidity gap (LRG) void of colour, which may serve as a signature. Note, though, that translating the above into a clean experimental procedure is not trivial. This issue is currently studied by an LHC working group.

Note: in actual analysis we relate to pseudorapidity

$$\eta = -\ln\left(\tan\frac{\theta}{2}\right)$$

2. Good-Walker Eikonal Models

Consider a system of two Fock states, a hadron Ψ_h and a diffractive state Ψ_D which are orthonormal. The GW mechanism stems from the observation that these states do not diagonalize the 2x2 interaction matrix $\mathbf{T}$. Introduce two wave functions Ψ_1 and Ψ_2 which diagonalize $\mathbf{T}$,

$$A_{i,k}^{i',k'} =< \Psi_i \Psi_k|\mathbf{T}|\Psi_{i'} \Psi_{k'} >= A_{i,k}\, \delta_{i,i'}\, \delta_{k,k'}. \tag{1}$$

i.e. the $A_{i,k}$ amplitudes are constructed from the elastic scatterings of Ψ_i and Ψ_k. In this representation the observed hadronic states are written

$$\Psi_h = \alpha\, \Psi_1 + \beta\, \Psi_2 \quad \Psi_D = -\beta\, \Psi_1 + \alpha\, \Psi_2\,, \tag{2}$$

where $\alpha^2 + \beta^2 = 1$. The corresponding unitarity equations are

$$Im\, A_{i,k}^S\,(s,b) = |A_{i,k}^S\,(s,b)\,|^2 + G_{i,k}^{in}(s,b), \tag{3}$$

where $G_{i,k}^{in}$ is the summed probability for all non GW inelastic processes induced by an initial (i,k) state. A general solution of Eq.(3) can be written as

$$1 - e^{-x} = 1 - x + \frac{x^2}{2!} + \frac{x^3}{3!} - \ldots$$

$$A_{i,k}^S(s,b) = i\left(1 - \exp\left(-\frac{\Omega_{i,k}^S(s,b)}{2}\right)\right), \tag{4}$$

$$G_{i,k}^{in}(s,b) = 1 - \exp\left(-\Omega_{i,k}^S(s,b)\right), \tag{5}$$

where $\Omega_{i,k}^S$ are arbitrary. In the eikonal approximation $\Omega_{i,k}^S$ are assumed to be real and determined by the Born (non screened) input. From Eq.(5) we deduce that the probability that the initial projectiles (i,k) reach the final LRG diffractive interaction unchanged, regardless of the initial state re-scatterings, is given by $P_{i,k}^S = \exp\left(-\Omega_{i,k}^S(s,b)\right)$. In general, we have to consider four possible (i,k) elastic re-scattering options. For initial p-p (or $\bar{p}$-p) the two off diagonal amplitudes are equal, $A_{1,2}^S = A_{2,1}^S$. The corresponding elastic, SD and DD amplitudes are

$$a_{el}(s,b) = i\{\alpha^4 A_{1,1}^S + 2\alpha^2\beta^2 A_{1,2}^S + \beta^4 A_{2,2}^S\}, \tag{6}$$

GW low mass

$$a_{sd}(s,b) = i\alpha\beta\{-\alpha^2 A_{1,1}^S + (\alpha^2 - \beta^2) A_{1,2}^S + \beta^2 A_{2,2}^S\}, \tag{7}$$

$$a_{dd} = i\alpha^2\beta^2\{A_{1,1}^S - 2A_{1,2}^S + A_{2,2}^S\}. \tag{8}$$

The eikonal model calculations exclusively depend on the input opacities where,

$$\Omega^S_{i,k}(s,b) = \nu^S_{i,k}(s)\Gamma^S_{i,k}(s,b,\alpha'_{I\!P})$$

$\nu^S_{i,k}(s) = g_i g_k (\frac{s}{s_0})^{\Delta_{I\!P}}$ and $\Gamma^S_{i,k}$ are the b-space profiles. In the GLMM model the (i,k) b-profile is given as the b-transform of a two pole t-profile ($t=-q^2$). Setting $\alpha'_{I\!P}=0$, the profiles are energy independent,

$$\frac{1}{(1\,+\,q^2/m_i^2)^2} \times \frac{1}{(1\,+\,q^2/m_k^2)^2} \implies \Gamma\left(b; m_i, m_k; \alpha'_{I\!P}=0\right).$$

A small energy dependence is introduced via

$$m_i^2 \implies m_i^2(s) \equiv \frac{m_i^2}{1\,+\,\alpha'_{I\!P}\ln(s/s_0)/4m_i^2}.$$

The Durham group (KKMR) has achieved similar output of $\frac{d\sigma_{el}}{dt}$ ($t \leq 0.5$ GeV) with a different profile which is numerically similar to ours.

2 recent models, based on the principles I have just outlined, obtain similar fits for pp and $\bar{p}p$ σ_{tot} and σ_{ee} ($t \lesssim 0.5\ GeV^2$) in the ISR-Tevatron range even though they are quite different in their modelling and data analysis procedures. An additional model yielding similar results is KMR (2000) in which the same data was tuned rather than fitted.

	Δ_{IP}	$\alpha'_{IP}(GeV^{-2})$	χ^2/dof
GLMM (2008)	0.12	0.012	0.87
L KMR (2009)	0.12	0.033	0.83
KMR (2000)	0.10	0.066	tuned

Note that all 3 models obtain α'_{IP} much smaller than $\alpha'_{IP}(DL) = 0.25\ GeV^{-2}$

Note that a small α'_{IP} output is not a general feature of eikonal models. It is induced by the choice of $\Gamma_{i,k}(s,b)$ which reproduce $d\sigma_{ee}/dt$ ($t \lesssim 0.5\ GeV^2$).

3. Multi Pomeron Interactions

GW models reproduce well the elastic amplitude but their SD and DD outputs considerably underestimate the experimental cross sections.
This deficiency is traced to high mass diffraction initiated to the lowest order by Mueller (1970) triple Pomeron diagram.

Consider a single diffraction channel $p + p \to p + M_{sd}$. Mueller's triple Pomeron mechanism, derived from 3 body unitarity, leads to high SD mass which is non GW. In the leading order

$$M_{sd}^2 \frac{d\sigma^{3I\!P}}{dt dM_{sd}^2} = \frac{1}{16\pi^2} g_p^2(t) g_p(0) G_{3I\!P}(t) \left(\frac{s}{M_{sd}^2}\right)^{2\Delta_{I\!P}+2\alpha'_{I\!P}t} \left(\frac{M_{sd}^2}{s_0}\right)^{\Delta_{I\!P}} . \qquad (12)$$

The virtue of Eq.(12) is that $\Delta_{I\!P}$ can be determined from either the energy or mass dependences of the SD cross sections. This approximation is valid for $s >> M_{sd}^2 >> m_p$.

CDF analysis suggests[8] a relatively large value of $G_{3I\!P}$. Consequently, we need to consider a very large family of multi Pomeron interactions (enhanced $I\!P$) which are not included in the GW mechanism. As we shall see, this "new" dynamical feature initiates profound differences in the calculated values of soft cross sections and non GW diffractive gap survival probabilities (soft and hard). Note that this features become significant above the Tevatron energy.

KMR (2007) and GLMM (2008) treatment of multi Pomeron interactions stems from Gribov Reggeon calculus utilized by Kaidalov et al. (1986). Recall, though, that KMR model is partonic, while GLMM is DQCD based.

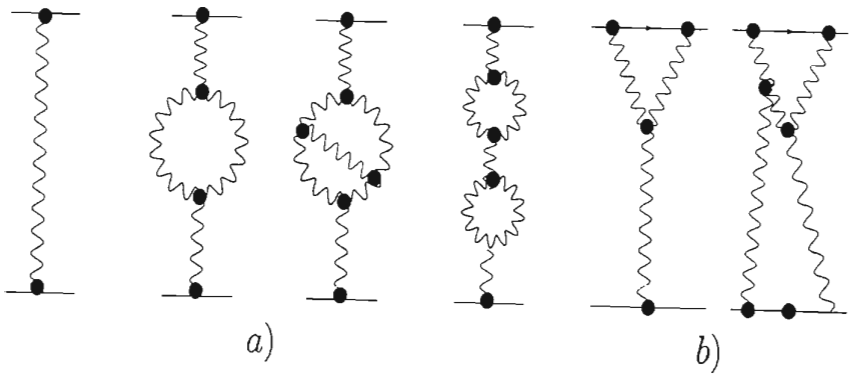

Typical low order terms of the Pomeron Green function.

a) Enhanced diagrams which renormalize the $\mathbb{P}$ propagator.
b) Semi Enhanced diagrams which renormalize the $\mathbb{P}$ vertex.

The partonic structure of the Pomeron derives from Gribov(1968) who associated $\alpha'_{\mathbb{P}} \simeq 1/\langle P_t^2 \rangle \cdot \langle P_t \rangle$ is the mean parton momentum. In our context we follow Mueller(1994, 1995) who showed that, in the large $N_c \gg 1$, the correct degree of freedom are colourless dipoles.

The data analysis I shall present supports a diminishingly small $\alpha'_{\mathbb{P}}$. This lends support to a typical large parton momentum $\langle P_t \rangle \simeq \frac{1}{\sqrt{\alpha'_{\mathbb{P}}}} \gtrsim 10$ GeV. This estimate implies that the running QCD coupling $\alpha_s \simeq 0.10 - 0.15$, hence GLMM pQCD Pomeron formalism which improves Gribov partonic

GLMM Pomeron formalism is based on 3 input assumptions:

1) $\alpha'_{I\!P} = 0$. This assumption is postulated also by KMR.
It implies that the soft Pomeron is hard enough to be treated perturbatively. The diminishing effect of $\alpha'_{I\!P}$ is compensated by a large $\Delta_{I\!P} \simeq 0.35$.
Recall that in hdQCD $\alpha'_{I\!P} \propto \frac{1}{Q_s(x)}$ in the small x limit.

2) GLMM pQCD calculations follow MPSI (1994, 1995) in which the exact Pomeron Green function is

$$N_{el}^{MPSI}(Y) = G_{I\!P}(Y) = 1 - \exp\left(\frac{1}{T(Y)}\right)\frac{1}{T(Y)}\,\Gamma\left(0, \frac{1}{T(Y)}\right).$$

$T(Y) = \gamma e^{\Delta_{I\!P} Y}$, $\Gamma(0,x)$ is the incomplete gamma function.
The MPSI approximation takes into account just the lowest order decay $I\!P \to 2\,I\!P$ and anihilation $2\,I\!P \to I\!P$.
Higher order $n\,I\!P \to m\,I\!P$ are reconstracted from triple $I\!P$ vertexes through Fan Diagrams.

KMR follow Kaidalov et al. (1986) assuming a point coupling for $n\mathbb{P} \to m\mathbb{P}$.

$$g_m^n = \tfrac{1}{2} g_N^{\,n\,m} \lambda^{n+m-2} = \tfrac{1}{2}\, n\, m\, G_{3\mathbb{P}}^{\,n+m-3}.$$

In this approximation $G_{3\mathbb{P}} = \lambda g_N$. λ is a free parameter. Note that Kaidalov et al. have a similar g_m^n definition with a different normalization.

3) The most critical difference between GLMM and KMR is that GLMM sum the enhanced diagrams, whereas KMR (following Kaidalov et al.) sum the semi enhanced diagrams. Obviously, a complete calculation should include both sets of diagrams. However, this is a non trivial undertaking. I shall return to this issue when discussing the output predictions of these models. An important technical comment: the semi enhanced diagrams are cardinal in SD calculations. They have been inserted by hand into the SD calculations of GLMM.

4. Survival Probabilities

The eikonal model explicitly provides the s-channel unitarity corrected elastic and GW diffractive amplitudes. The survival probability S^2 is defined (Bjorken (1992), GLM(1993, 1995)) as a soft damping factor applicable to non GW diffractive cross sections commonly identified by a LRG signature.

For exclusive diffraction
$$S^2_{2ch}(s) = \frac{\int d^2b \left| \sum_{i,k} \left(M_{diff}(s,b) \exp\left(-\tfrac{1}{2}\Omega^s_{i,k}(s,b)\right)\right|^2}{\int d^2b \left| M_{diff}(s,b)\right|^2}.$$

Recall that $P^s_{i,k}(s,b) = \exp\left(-\Omega^s_{i,k}(s,b)\right) = \left(1 - A^s_{i,k}(s,b)\right)^2$ is the probability that the initial colliding projectiles (i,k) reach the final diffractive interaction unchanged regardless of their initial re-scatterings.

Even though GLMM and KMR eikonal models are not identical, their outputs are compatible.

Multi Pomeron interactions provide additional damping of the elastic and diffractive channels, reflecting t-channel unitarity constraints. The s and t channel dampings are factorizable $S^2 = S^2_{2ch} \times S^2_{enh}$. Note that S^2 is channel dependant.

In the GLMM S^2_{enh} is calculated utilizing the MPSI approximation. After some algebra we obtain:

$$\langle |\, S^2_{enh}\,(MPSI)\,| \rangle\,(Y) \;=\; = S\,(\mathcal{T}(Y)) \;-\; 2\,e^{-\Delta_{I\!P}(Y-\delta Y_H)/2}\,S1\,(\mathcal{T}(Y)) \;+\; e^{-2\Delta_{I\!P}(Y-\delta Y_H)/2}\,S2\,(\mathcal{T}(Y));$$

$$S(T) = \frac{1}{T^3}\left\{-T \;+\; e^{\frac{1}{T}}\;(1+T)\;e^{\frac{1}{T}}\;\Gamma\left(0,\frac{1}{T}\right)\right\};$$

$$S1(T) = \frac{1}{T^3}\left\{-T(1+T) \;+\; (1+2T)\,e^{\frac{1}{T}}\;\Gamma\left(0,\frac{1}{T}\right)\right\};$$

$$S2(T) = \frac{1}{T^3}\left\{T\left[(T-1)^2-2\right] \;+\; (1+3T)\,e^{\frac{1}{T}}\;\Gamma\left(0,\frac{1}{T}\right)\right\}.$$

where

$$\mathcal{T}\,(Y) \;=\; \gamma\left(e^{\Delta_{I\!P}(Y-Y')}-1\right)\left(e^{\Delta_{I\!P}Y'}-1\right).$$

As we saw KMR Pomeron enhancement model is different. In the KMR model S^2_{enh} is much larger than estimated by GLMM. I shall discuss these 2 sets of predictions in the next section.

A reliable estimate of S^2 is essential for realistic predictions of inelastic hard diffraction rates at the LHC. Of particular interest is central exclusive diffractive Higgs production: $P+P \to P+LRG+H+LRG+P$.

When the final protons are tagged this channel has the advantage of a 2 LRG signature and a good signal to background ratio. The counting rate of this channel depends on S^2. GLMM calculation of S^2 shows S^2_{enh} to be an order of magnitude smaller than S^2_{2ch}.

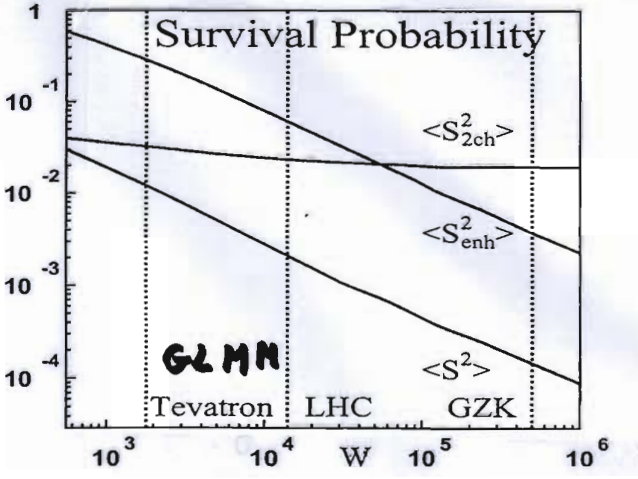

5. The Interplay Between Data and Theory

5.1 Procedures: GLMM data base contains 55 points (σ_{tot}, σ_{el}, σ_{sd}, σ_{dd}, B_{el}) in the ISR-Tevatron energy range. The data was fitted so as to extract the Pomeron parameters.

CDF 1800 GeV data on $\frac{d\sigma_{el}}{dt}$ ($t \leq 0.5$ GeV^2) and $\left.\frac{d\sigma_{sd}}{dt\, dM^2_{sd}}\right|_{t=0.05}$ were satisfactory reproduced as predictions of the model.

There is a significant difference between the fitting procedure carried out by GLMM and KMR/L4MR. We have fitted our data base with a GW model reproducing the elastic amplitude well but considerably underestimative the SD and DD cross sections. We have then repeated the fit with our GW+IP-enh model obtaining a good reproduction of the entire data base (including the CDF 1800 GeV data). Comparing the 2 fits we note that α'_{IP} outputs are stable while Δ_{IP} changes from 0.12 to 0.335

Δ_{IP}(L4MR) = 0.12 (GW)

	Δ_{IP}	β	α'_{IP} GeV^{-2}	g_1 GeV^{-1}	g_2 GeV^{-1}	m_1 GeV	m_2 GeV	χ^2/d.o.f.
GW	0.120	0.46	0.012	1.27	3.33	0.913	0.98	0.87
GW+$I\!P$ − enh.	0.335	0.34	0.010	5.82	239.6	1.54	3.06	1.00

Δ_{IP} (4MR07) = 0.5

Δ_{IP} (4MR08) = 0.3

We also observe that the GW couplings $\frac{g_2}{g_1} = O(1)$ in the GW fit. Once Pomeron enhancement is included $\frac{g_2}{g_1} \gg 1$. This large ratio implies that the elastic amplitude approach toward the black bound is very slow. KMR/LKMR adjusted in the 1st stage their GW parameters from the elastic data sector. These parameters were fed as fixed input into the 2d stage in which the $\mathbb{P}$ enhanced parameters were adjusted. KMR/LKMR assume that $g_1 \approx g_2$ which implies a fast approach to the black bound - just above the LHC top energy.

5.2 Predicted cross sections:

GLMM and KMR (07)/(08) predicted cross sections are presented below. KMR (08) construct the Pomeron as a superposition of 3 input Pomerons.

	Tevatron			LHC			$W=10^5$ GeV		
	GLMM	KMR(07)	KMR(08)	GLMM	KMR(07)	KMR(08)	GLMM	KMR(07)	KMR(08)
σ_{tot}	73.3	74.0	73.7	92.1	88.0	91.7	108.0	98.0	108.0
σ_{el}	16.3	16.3	16.4	20.9	20.1	21.5	24.0	22.9	26.2
σ_{sd}	9.8	10.9	13.8	11.8	13.3	19.0	14.4	15.7	24.2
σ_{dd}	5.4	7.2		6.1	13.4		6.3	17.3	
$\frac{\sigma_{el}+\sigma_{diff}}{\sigma_{tot}}$	0.43	0.46		0.42	0.53		0.41	0.57	

a) Total and elastic cross sections predicted by GLMM and KMR(08) are essentially identical.

b) Both KMR models predict diffractive cross sections consistently larger than GLMM. The difference increases with energy. Note that the definitions of low and high mass diffraction are somewhat different in GLMM and KMR. KMR(08) predicts only the low mass value of σ_{dd}.

c) A dramatic moderation of σ_{tot} and σ_{el} increase with energy is predicted above the Tevatron by the 3 models. This is a direct consequence of the Pomeron renormalization.

Tev range	$\Delta_{IP}^{eff}(\sigma_{tot})$	$\Delta_{IP}^{eff}(E)$
0.9–3.5	0.066	0.079
3.5–7.0	0.056	0.058
7.0–14.0	0.049	0.050
14.0–100.0	0.041	0.035

GLMM

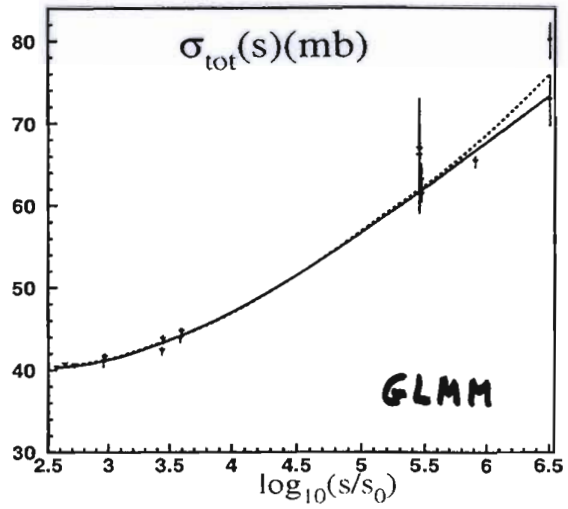

Recall that Δ_{IP} is an input to models with screening initiated by eikonalization and multi-Pomeron interactions. A good measure of the predicted energy dependence is by checking Δ_{IP}^{eff}. Recall that Δ_{IP}^{eff} is channel dependent.

Experimental verification (or rejection) of the cross section predictions I have just presented is expected at a relatively early stage of the LHC operation. At 7 Tev GLMM predict:

σ_{tot} = 86.0 mb
σ_{el} = 19.5 mb

to be compared with 90-100 mb, no PP-enh.
23-26 mb

5.3 Survival Probabilities: In the table below I present the GLMM and KMR calculated survival probabilities for exclusive central diffractive standard Higgs (120-160 GeV).

	Tevatron			LHC (14 TeV)			$W=10^5$ GeV		
	GLMM	KMR(07)	KMR(08)	GLMM	KMR(07)	KMR(08)	GLMM	KMR(07)	KMR(08)
$S^2_{2ch}(\%)$	5.3	2.7-4.8		3.9	1.2-3.2	4.5	3.2	0.9-2.5	
$S^2_{enh}(\%)$	28.5	100		6.3	100	33.3	3.3	100	
$S^2(\%)$	1.51	2.7-4.8		0.24	1.2-3.2	1.5	0.11	0.9-2.5	

At 7 TeV S^2 = 0.6 % (GLMM)

S^2_{2ch} as obtained in the 3 models are compatible within the uncertainties of these calculations.

GLMM calculation of S^2_{enh} is considerably smaller than KMR. This is traced to the different summations of the multi Pomeron interactions. The smaller S^2_{enh} in GLMM imply stronger Pomeronic screening than in KMR. This may explain why KMR diffractive cross sections are consistently higher than GLMM.

Preliminary Tel-Aviv calculations sugest that S^2_{enh} in which both enhanced and semi-enhanced diagrams are summed is equate to the original value obtained in GLMM. This resuets supports KMR(07) calculations in which their $S^2_{enh} \simeq 1$.

5.4 Single xlusive production of charged particles:

The first round of Alice, CMS and ATLAS LHC measurements provided information on $\frac{1}{\sigma_{in}} \frac{d\sigma_{inc}}{d\eta}$ at 0.9, 2.36, 7.0 TeV.

Analysis of this channel is a natural extention of the GLMM model entailing 3 additional parameters: 2 coefficients $a_{\pi\pi}, a_{\gamma}$

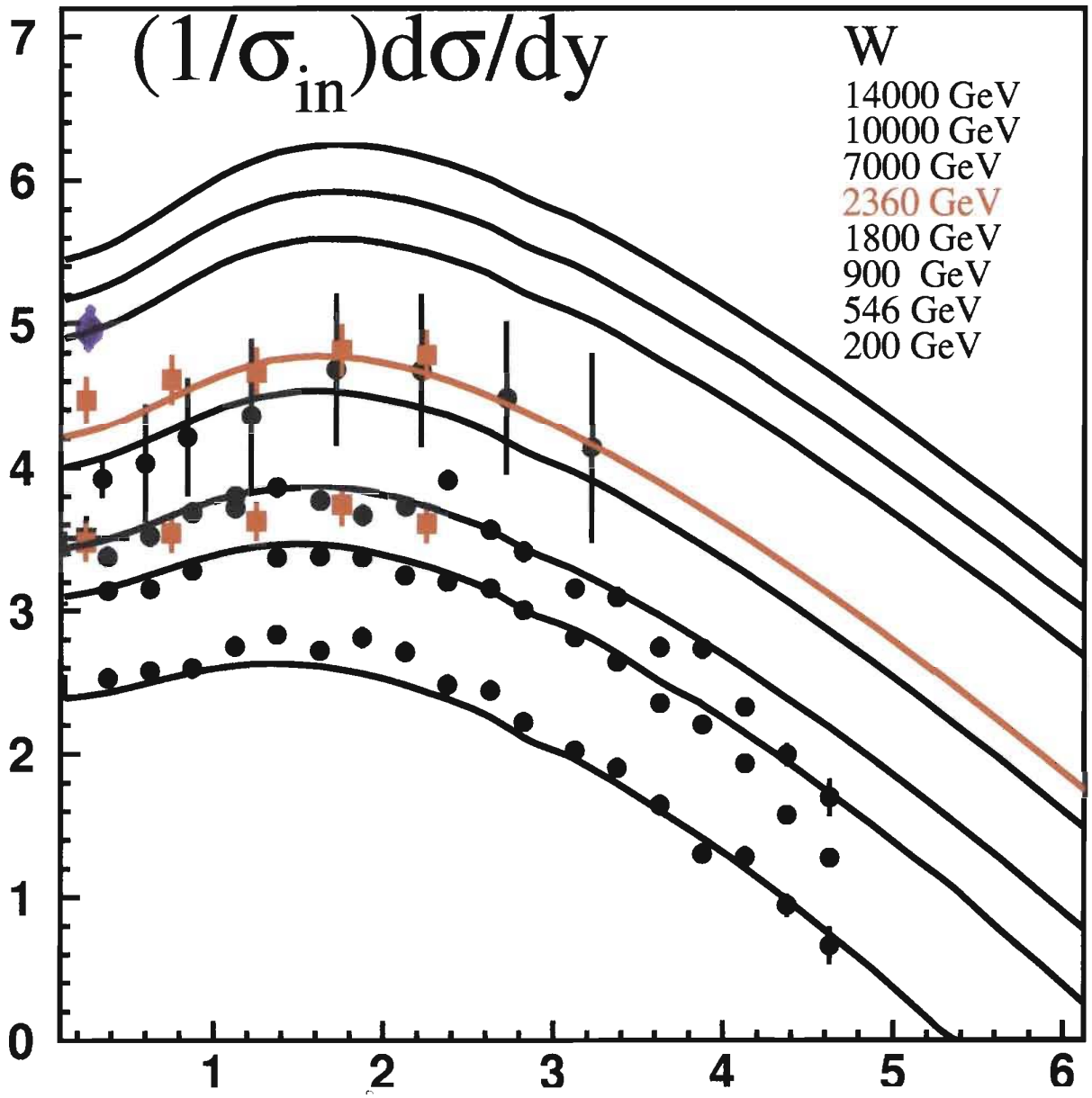

to which we add a dimensional parameter Q needed to trasform the rapidity y to pseudorapidity η.

The figure is our fitted data reproductio at 200-1800 Gev to which we have added the LHC data imposed on our predictions. Note that Alice point at 7 Tev was re scaled by us to conform with the normalization of the low energy data.